# Towards the Minimum Inner Edge Distance of the Habitable Zone

Andras Zsom, Sara Seager, Julien de Wit

Department of Earth, Atmospheric and Planetary Sciences, Massachusetts Institute of Technology, Cambridge, MA 02139, USA; zsom@mit.edu

Received _____; accepted _____

## ABSTRACT

We explore the minimum distance from a host star for an exoplanet to be potentially habitable, in order to maximize future chances of finding other habitable worlds. We find that the inner edge of the Habitable Zone (HZ) for hot desert worlds is at 0.5 AU around a solar-like star (well within the orbit of Venus). The relative humidity is the key controlling factor in determining the inner edge distance because water vapor has a strong impact on the greenhouse warming of the atmosphere, yet too little water vapor will deactivate precipitation and enable $CO_2$ to accumulate. We estimate that a relative humidity as low as 1% can be sufficient to maintain a liquid water cycle and wash out $CO_2$ from the atmosphere. If the surface pressure is too low ($\sim$0.1 bar), the water loss timescale of the planet is too short to support life. If the surface pressure is too high ($\sim$100 bars), we show using atmospheric circulation arguments, that the day-night side temperature difference on slow rotators and tidally locked planets is too small to enable an active water cycle. In contrast, the temperature difference on fast rotators with high surface pressure can be large enough to produce rain. Intermediate surface pressures ($\sim$1-10 bars) can provide suitable conditions for a water cycle independent of the planetary rotation period. We additionally find that the water loss timescale is influenced by the atmospheric $CO_2$ level, because it indirectly influences the stratospheric water mixing ratio. If the $CO_2$ mixing ratio of dry planets at the inner edge is smaller than $10^{-4}$, the water loss timescale is $\sim$1 billion years, which may be too short for complex life to evolve. Hot desert worlds might be identified using transmission spectroscopy and atmospheric retrieval methods. A hot desert world has small amounts of greenhouse gases (water and $CO_2$) in the stratosphere, and the background gas must be optically inactive in the mid-infrared. The new inner edge limit is significantly closer

to the host star than previous estimates. Therefore, the number of potentially habitable confirmed/validated planets increases by a factor of 2-3.

*Subject headings:* ...

## 1. Introduction

One of the main driver of exoplanet sciences is to find habitable or inhabited exoplanets. By definition an exoplanet is habitable if liquid water, a crucial ingredient for life, is present on its surface, and if the surface temperature and pressure are such that complex organic molecules are stable (Lang 1986). Habitability is inferred remotely by studying the atmosphere of exoplanets and retrieving atmospheric physical conditions such as the temperature profile and composition (Benneke & Seager 2012), or more specifically the presence of biosignature gases (e.g., Des Marais et al. 2002; Segura et al. 2005; Kaltenegger et al. 2010; Sterzik et al. 2012). Surface properties might be retrievable if the atmosphere is optically thin in so-called window regions of the spectrum. For example, if the surface pressure is small and the atmosphere is not fully covered by clouds, the surface properties are retrievable (e.g., Seager et al. 2005; Fujii et al. 2011; Hegde & Kaltenegger 2013).

We summarize highlights of previous work on the inner edge of the Habitable zone going from the smallest to the largest inner edge distance. Typically an Earth-like planet with an Earth-like atmosphere is studied, by changing one attribute at a time. We describe this attribute and the level of model complexity. The inner edge around a solar-like star is located at 0.77 AU for an Earth-like planet with a limited water reservoir based on 3D global circulation models (Abe et al. 2011). Vladilo et al. (2013) showed using an energy balance model and varying the surface pressure between 0.3 and 3 bars that the inner edge is located at 0.85 AU within the parameter range where their model is calibrated. By maximizing the cooling effect of clouds on an Earth-like planet, the inner edge could be located as close as 0.87 AU around the Sun based on 1D models with clouds (Kitzmann et al. 2010). 1D cloud-free calculations show that the inner edge is at 0.88 AU for an Earth-like planet with 10 bar $N_2$ (Kasting et al. 1993). These calculations have been redone with updated

opacity data (Kopparapu et al. 2013). The new results show that the inner edge is 0.92 AU assuming an Earth-like atmosphere on a super-Earth planet[1].

Here, we find that the inner edge is much closer to the host star, when non-Earth-like atmosphere conditions are considered. Super-Earth and Earth-sized planets are expected to be diverse and an extension of diversity to atmospheres must be considered in habitability studies, if we want to maximize our chances of finding a habitable world. We must first identify the key parameters influencing habitability and then establish the broadest (but plausible) range where the parameters could reside. In this work, the extreme value is adopted for some parameters, and the full range is considered for others. We use a variety of methods to estimate habitability: we calculate 1D radiative-convective temperature-pressure and mixing ratio profiles; we study the effect of atmospheric circulation on the climate using order of magnitude estimates; and we also calculate the water loss timescale (the length of time over which the planet loses its water reservoir). All these methods are combined to identify the atmospheric scenarios that minimize the inner edge distance, and to reject scenarios where the planet is not hospitable for life.

The inner edge of the habitable zone is controlled mainly by the properties of the host star, the planet atmosphere's relative humidity, $CO_2$ mixing ratio, the most abundant gas, and the surface pressure. The first order effect of the host star is related to the inverse square law. The stellar luminosity increases with stellar mass, therefore the habitable zone is more distant around massive stars (Kasting et al. 1993). The atmospheric relative humidity is controlled by the water cycle. The $CO_2$ mixing ratio is affected by the carbon-silicate cycle as well as the water cycle (both cycles are discussed in detail in the next paragraph). The most abundant gas of close-in habitable exoplanets is expected to be optically inactive, e.g., not a greenhouse gas, and not $H_2$ because $H_2$ is a potent

[1]The calculation with the 10 bar $N_2$ atmosphere was not performed in the new study.

greenhouse gas due to collision induced absorption (Pierrehumbert & Gaidos 2011). The surface pressure is determined by various processes including (but not limited to) accretion from the protoplanetary disk, outgassing, atmospheric escape, accretion/erosion during impacts. Other aspects such as e.g., clouds (Kitzmann et al. 2010; Goldblatt & Zahnle 2011; Zsom et al. 2012, e.g.,), tidal heating (Barnes et al. 2012), and the surface albedo at low surface pressures (Joshi & Haberle 2012) could also impact the inner edge distance.

The water cycle and the carbon-silicate cycle are the two most important processes that can alter the atmospheric composition and the surface pressure, and so we discuss it in more detail. The water cycle provides a positive climate feedback. As the surface becomes warmer, the evaporation rate of the surface waters increase and water vapor builds up in the atmosphere. As the optical depth of the atmosphere increases with the water mixing ratio, the greenhouse effect becomes stronger promoting further warming and evaporation (see e.g., Goldblatt & Watson 2012, and references therein). The carbon-silicate cycle is a climate stabilizer feedback process operating on a $10^6$ years timescale (Walker et al. 1981). $CO_2$ is removed from the atmosphere by liquid water precipitation and surface weathering of silicate rocks (Abbot et al. 2012). The weathered rocks are transported to oceans where abiotic or biotic processes produce $CaCO_3$ that sediments to the sea floor. If plate tectonics is present on the exoplanet, $CaCO_3$ is subducted to the mantle and removed from the surface regions. $CO_2$ reforms by metamorphism in the mantle and it is outgassed by volcanism that closes the carbon-silicate cycle. If the climate cools, liquid precipitation (a sink for atmospheric $CO_2$) is reduced, therefore $CO_2$ builds up in the atmosphere and warms the surface to a new equilibrium temperature. The width of the Habitable Zone (HZ) is affected by these two cycles for an Earth-like planet (Kasting et al. 1993; Kopparapu et al. 2013).

We do not model the outer edge of the Habitable Zone, because previous work suggests

that even free-floating planets could be habitable (Stevenson 1999). In other words, the outer edge of the Habitable Zone is at infinity. Such planets must have a thick $H_2$ atmosphere to reduce the outgoing thermal emission and allow for slow cooling. Habitable conditions can also be maintained for an extended period of time, if heat is generated in the interior of the planet by e.g., radioactive decay (Rogers&Seager, in prep.).

The paper's outline is the following. In Sect. 2, we first describe the initial atmosphere profiles and how the convective tropospheric temperature-pressure profile is calculated (Sect. 2.1). Then we introduce our climate code specifically developed for this study (Sect. 2.2). We describe the influence of atmospheric parameters on the inner edge distance in Sect. 2.3. We develop atmospheric dynamics tools to assess the plausibility of best case scenarios in Sect. 2.4, and estimate the loss timescale of surface waters in Sect. 2.5. Our results are outlined in Sect. 3, where we present our main findings and supporting arguments. In Sect. 4, we discuss the formation and the observable signatures of hot desert worlds, and the model uncertainties. Finally we summarize our results and draw conclusions in Sect. 5.

## 2. Methods

Our aim is to find atmospheric configurations that provide habitable surface conditions as close as possible to the host star. We do this in three steps: first, we study how various atmospheric and planetary properties influence the location of the inner edge by calculating radiative-convective equilibrium temperature-pressure profiles (Sections 2.1, 2.2, and 2.3); second, we estimate the requirements for a water cycle because liquid water precipitation, surface weathering and volcanic outgassing regulates the atmospheric $CO_2$ level (Sect. 2.4); and third, we estimate the water loss timescale to determine whether the surface water reservoir is stable on a multi-billion year timescale (Sect. 2.5).

### 2.1. Initial atmospheric profiles and convection

The T-P profile and volume mixing ratios are initialized with a convective zone that follows the moist adiabat from the surface to the tropopause and is prolonged with an isothermal stratosphere. The atmosphere is described by the surface conditions (pressure, temperature, and albedo), relative humidity, $CO_2$ mixing ratio, background gas (typically $N_2$), and planetary surface gravity. Unless otherwise stated, we use 60 layers per pressure decade. The top-of-atmosphere pressure is fixed at $10^{-4}$ bar because the atmosphere is optically thin in all spectral bands above this level. The surface pressure is varied between 0.1 and 100 bars. First, we establish the mixing ratios of $CO_2$ and the background gases on a dry pressure grid (without water vapor). We assume that these gases are well mixed in the atmosphere and their mixing ratios are constant as a function of pressure. Next, the moist adiabat is built from the surface upwards given the dry surface pressure ($P_{\mathrm{surf,\,dry}}$), temperature ($T_{\mathrm{surf}}$), and relative humidity ($\Phi$) following Pierrehumbert (2011):

$$\frac{d\ln T}{d\ln P_{\mathrm{dry}}} = \frac{R_{bg}}{c_{p,\,bg}} \frac{1 + \frac{L}{R_{bg}T} f_{H_2O}}{1 + \left[\frac{c_{p,\,H_2O}}{c_{p,\,bg}} + \left(\frac{L}{R_{H_2O}T} - 1\right)\frac{L}{c_{p,\,bg}T}\right] f_{H_2O}}, \tag{1}$$

where $R_{bg}$ and $R_{H_2O}$ are the specific gas constant of the background gas and water vapor, respectively; $c_{p,\,bg}$ and $c_{p,\,H_2O}$ are the specific heat capacity of the background gas and water vapor, respectively; $L$ is the latent heat of water vapor, and $f_{H_2O}$ is the water vapor mass mixing ratio:

$$f_{H_2O} = \frac{m_{H_2O}}{m_{bg}} \frac{\Phi P_{\mathrm{sat}}(T)}{P_{\mathrm{dry}}}, \tag{2}$$

where $m_{bg}$ and $m_{H_2O}$ are the molecular masses of the background gas and water vapor, respectively, and $P_{\mathrm{sat}}(T)$ is the saturation vapor pressure at temperature $T$ calculated according to the Smithsonian Meteorological Tables. The moist adiabat is followed until the temperature drops below the prescribed initial stratosphere temperature. The stratospheric water vapor mixing ratio is constant and it is determined by the tropopause temperature

and relative humidity. Finally, the total atmospheric pressure is calculated as the sum of the water vapor partial pressure and the dry pressure.

### 2.2. Radiative-convective equilibrium profiles

We want to determine the equilibrium planet-star separation for given surface temperature and pressure. Therefore, we develop a specific numerical approach to calculate the T-P profiles: we fix the surface temperature and determine the semi-major axis where the atmosphere is in radiative equilibrium. Our approach solves the inverse climate problem, because typically the exoplanet's semi-major axis is fixed and the corresponding surface temperature is calculated (see e.g., the EXO-P model of Kaltenegger & Sasselov 2010).

The equilibrium T-P profile is determined by iterating the following steps:

- We calculate the fluxes propagating through each atmospheric layer in several wavelength bands, we treat the thermal emission of the exoplanet/atmosphere and the stellar irradiation separately, and evaluate the stellar irradiation fluxes at an arbitrary distance.
- We determine the semi-major axis where the top-of-atmosphere fluxes are in equilibrium using the Bond albedo of the exoplanet and the outgoing long wave radiation.
- The stellar irradiation fluxes are rescaled such that the incoming stellar flux corresponds to the value received at the new semi-major axis.
- The stratosphere temperature profile is updated based on the net fluxes propagating through the layers.
- The tropopause height is updated if necessary.

The iteration stops, when the T-P profile reaches equilibrium. These steps are described in the following.

### *2.2.1. Radiative transfer*

Fluxes are calculated in a limited number of wavelength bands for computational efficiency. The bands range between 0.2 to 200 microns, and they are linearly spaced in $\log(\lambda)$. Such spacing ensures that Planck functions of various temperatures are resolved with the same power. We use 400 wavelength bands. The sufficient number of bands were determined by convergence tests where the outgoing IR flux of a test atmosphere was monitored as the number of bands is gradually increased.

We calculate the optical depth of each layer in each wavelength band given the mixing ratio profiles. Various absorption and scattering sources could contribute to the optical depth of a layer. These are the greenhouse gas absorption (discussed in the next paragraph), Rayleigh scattering (Harvey et al. 1998; Weber 2003; Sneep & Ubachs 2005), UV absorption of $O_2$ and $O_3$ (Sander et al. 2006), collision induced absorption (CIA) of $H_2$ (Borysow 2002), $N_2$ (Borysow 2002), and $CO_2$ (Gruszka & Borysow 1997), and continuum absorption of water and $CO_2$ (following the description of Pierrehumbert 2011, Sect. 4.4.8). It is also possible to place cloud particles in the atmosphere. In that case, the absorption and scattering coefficients, and the asymmetry parameter of spherical droplets are calculated and tabulated using the Mie code of Bohren & Huffman (1983).

We use the line-by-line HITRAN database (Rothman et al. 2009) and the exponential sums formalism (Wiscombe & Evans 1977; Pierrehumbert 2011) to determine the band-averaged transmission through an atmospheric layer due to greenhouse gas absorption. The high resolution line-by-line absorption coefficient is calculated at a pressure and

temperature grid covering typical values encountered in our atmosphere profiles. We use the semi-analytical Voigt line profile of Liu et al. (2001), and determine the Voigt line width using the Doppler and Lorentz line widths (Olivero 1977). The histogram of absorption coefficients are pre-calculated and tabulated, and these tables are read and interpolated at run-time to the pressure and temperature values of each layer.

Once the optical depth of the atmosphere is known, fluxes propagating through the layer interfaces are calculated. We use the two-stream approximation and adopt the quadrature method for the stellar illumination, and the hemispheric mean approximation for the thermal radiation (Toon et al. 1989). The thermal flux of the planetary surface and atmosphere are treated separately from stellar irradiation. The distinction of the two fluxes is important to determine the equilibrium distance of hot inner edge planets with $T_{\rm surf} \sim$ 400-500 K orbiting low temperature M stars ($T_{\rm eff} \sim$ 2000-3000 K). The outgoing thermal emission of the planet and atmosphere might overlap with the reflected stellar light in the near-IR. However, it is necessary to determine the relative contribution of these fluxes determine the equilibrium distance of the planet (see Eq. 3).

### *2.2.2. Climate model*

The goal of the climate code is to iterate the temperature and water vapor profiles to a radiative-convective equilibrium based on the fluxes propagating through the layer interfaces. This is achieved in three stages. First, we determine the planet-star separation where the top-of-atmosphere incoming and outgoing fluxes are in equilibrium, and rescale the stellar fluxes using the new distance. Then we update the stratospheric temperature profile, and finally the tropopause height is determined. All steps are outlined below.

The distance where the top-of-atmosphere fluxes are balanced is calculated as

$$OTE = \frac{1}{4}(1-\alpha)F_{in}(a), \tag{3}$$

where $OTE$ is the top-of-atmosphere outgoing thermal emission, $\alpha$ is the Bond albedo of the planet, and $F_{in}$ is the top-of-atmosphere incoming stellar irradiation. As the T-P and mixing ratio profiles are assumed constant within one iteration, the outgoing thermal emission is independent of distance $a$. The albedo (the ratio of top-of-atmosphere outgoing and incoming stellar fluxes) is also distance-invariant, and it is evaluated at an arbitrary distance typically where the incoming stellar flux equals the Solar constant. Therefore, the unknown in Eq. 3 is $F_{in}$ and the distance $a$ where $F_{in}$ is received at the top of the atmosphere. Once the equilibrium incoming stellar flux is determined, the downwelling and upwelling stellar fluxes are renormalized.

We update the stratospheric temperature in the next step. We adopt a numerically efficient and simple approach to update the T-P profile: the temperature of a layer is increased by $dT$, if the net flux propagating through the layer ($dF_i$ - the difference between incoming and outgoing fluxes) is positive, and the temperature decreases otherwise. The temperature step ($dT$) is 0.5 K in our simulations. Our method differs from traditional approaches that calculate the derivative $dT_i/dt$ (change of temperature over time) in each atmospheric layer $i$:

$$\frac{dT_i}{dt} = \frac{g}{c_{pi}}\frac{dF_i}{dP_i}, \tag{4}$$

where $g$ is the gravitational constant, $c_{pi}$ is the total heat capacity of the layer, $dF_i$ is the net flux propagating through the layer, $dP_i$ is the pressure difference at the top and bottom of the layer. If the net flux is negative, the layer cools. The time step ($dt$) is adaptively determined by setting an upper limit on $dT_i$ ($dT_{max}$). We find that although the traditional approach properly captures how the temperature profile evolves in time, it converges slowly if the tropopause pressure level is orders of magnitude larger than the top-of-atmosphere

pressure level. Furthermore, it is unimportant how the temperature profile evolves in time from an arbitrary initial state, as the goal is to determine an equilibrium profile.

Finally, the tropopause height and the stratospheric water mixing ratio is updated in the climate code. The lapse rate between the tropopause layer and the layer above is calculated. The tropopause height is increased by one layer, if the lapse rate is steeper than the moist adiabat. The tropopause height is decreased by one layer, if the lapse rate is larger than 0 K/km (i.e., the layer above the tropopause is warmer). As the tropopause temperature changes, so does the tropopause and stratospheric water mixing ratios.

The steps outlined in the previous two sections, namely radiative transfer, determining the equilibrium distance, stratosphere temperature, tropopause, and water mixing ratio updates, are iteratively performed until the temperature profile relaxes to equilibrium. Our convergence criteria measures the temperature change of each layer for $n$ iterations. Convergence is reached, if the temperature change is less than $2\,dT$ in all of the layers during $n$ successive iterations, where $n$ is typically 10. Model validation and tests are described in App. A.

### 2.3. The ranges of model parameters, and their effect on the inner edge

We provide a qualitative description on how the various atmospheric parameters influence the outgoing thermal flux, the albedo of the planet, and thus the inner edge distance in this section. In general, increasing the outgoing thermal emission and/or the albedo of the planet moves the inner edge closer to the star because more incoming stellar flux is necessary to achieve radiative-convective equilibrium. The most important effects of these parameters is described in detail in Sect. 3, while other parameters are fixed during the simulations.

**Stellar type** We perform simulations using various stellar types ranging from M6V to F0V, or from 3000 K to 7200 K effective temperatures (Castelli & Kurucz 2004). The first order effect of stellar type is related to the luminosity of main sequence stars. An exoplanet has to be much closer to an M dwarfs than to an F star to receive the same total flux at the top of its atmosphere. However, the spectral energy distribution of stars have higher order effects on the inner edge distance. These effects become apparent, if the top-of-atmosphere fluxes are compared at the inner edge around various stars (Kopparapu et al. 2013). The spectral energy distributions (SEDs) of low mass stars peak at longer wavelengths where Rayleigh scattering is less efficient, thus the planetary albedo is reduced. Furthermore, a larger fraction of the incoming stellar radiation is directly absorbed by the atmosphere around low mass stars because the greenhouse gases such as $H_2O$ and $CO_2$ absorb in the near IR. To a smaller extent, the UV flux of the host star (especially the extreme UV) influences the composition of the stratosphere, which in turn can slightly influence the surface climate (see Fig. 4a of Rugheimer et al. 2012).

**Surface gravity** The effects of surface gravity are two-fold. If the surface pressure is fixed, the cumulative optical depth of the atmosphere is reduced at all wavelengths for a larger surface gravity because the atmospheric scale height and thus the column density of greenhouse gases are reduced. On one hand, this increases the outgoing thermal emission of the exoplanet and shifts the inner edge closer to the star. On the other hand, more stellar flux reaches the surface because less stellar flux is absorbed by the atmosphere, and the column density of Rayleigh scattering background gas is reduced. If the surface albedo is low, the Bond albedo of the planet is reduced and the inner edge is pushed further away from the star. If the surface is reflective, the inner edge is pushed closer to the star. Therefore the albedo-effect of surface gravity depends on the relative contributions of two effects to the Bond albedo: Rayleigh scattering, and surface reflection. The mass and

radius of an exoplanet also influences how much atmosphere can the planet retain (see e.g., Lammer et al. 2009), and what is the volatile content of the mantle that can potentially be outgassed.

We use values between $g = 5$ m/s$^2$ for a planet somewhat larger than Mars, 10 m/s$^2$ for an Earth-like planet, and 25 m/s$^2$, which is a typical surface gravity of a 10 $M_{\rm Earth}$ super-Earth.

**Surface pressure** The effect of surface pressure on the inner edge distance is two-fold. Larger surface pressure increases the albedo of the planet due to Rayleigh scattering. However, an increasing surface pressure also raises the column density of the greenhouse gases and thus the cumulative optical depth of the atmosphere for a fixed the mixing ratio. Therefore, the effect of surface pressure on the inner edge distance cannot be readily estimated, thus we treat it as a free parameter. We consider planets with 0.1, 1, 10, and 100 bars of surface pressure.

**$CO_2$ mixing ratio** The lower the $CO_2$ mixing ratio is, the closer the inner edge of the HZ is to the star. $CO_2$ in combination with water vapor is a very effective greenhouse gas because these gases have non-overlapping absorption bands in the infrared. If $CO_2$ was removed from the atmosphere of Earth, the global average temperature would be below the freezing point of water (Pierrehumbert 2011). Therefore it is crucial to calculate how the mixing ratio of $CO_2$ influences the inner edge distance.

The atmospheric $CO_2$ level is determined by the balance between the sources and sinks of $CO_2$. The abiotic source of $CO_2$ is outgassing from the planetary interior. $CO_2$ is removed from the atmosphere by liquid water precipitation followed by silicate weathering (Walker et al. 1981). Atmospheric $CO_2$ is converted into carbonates during the weathering

process. The carbonates can either dissolve in water as they sediment at deep ocean regions, or accumulate in solid form at shallow water regions. The role of plate tectonics in the carbon-silicate cycle is to recycle carbon. Plate tectonics removes the carbonates from the shallow water regions by subduction and $CO_2$ reforms at the high temperatures of the mantle. Later $CO_2$ is outgassed by volcanism that closes the carbon-silicate cycle.

If an exoplanet has no plate-tectonics but volcanism and surface weathering, carbonates can accumulate in the shallow water regions until the mantle becomes devoid of $CO_2$. As the source of $CO_2$ at this point is depleted, liquid precipitation in combination with surface weathering can remove all $CO_2$ from the atmosphere. The timescale of complete atmospheric $CO_2$ removal on Earth is estimated to be 400 million years (Kasting et al. 1993). The timescale over which the mantle becomes carbon-free depends on the $CO_2$ outgassing rate and the carbon content of the interior. By various estimates, the mantle of Earth holds $6 \times 10^{17}$ - $4 \times 10^{20}$ kg of carbon (Javoy et al. 1982; Sleep & Zahnle 2001; Coltice et al. 2004). The outgassing rate of $CO_2$ is $3.3 \times 10^{11}$ kg/year (Walker et al. 1981). Given these estimates, the carbon depletion timescale of Earth's mantle could be anywhere between $10^6$ and $10^9$ years, which is at least an order of magnitude shorter than the main-sequence life of the Sun. Therefore an exoplanet with an active hydrological cycle but no plate tectonics could be $CO_2$-free, unless $CO_2$ sources other than volcanism exist on the planet.

The presence of plate tectonics on exoplanets is difficult to asses both observationally or theoretically. Our current understanding is that it is less likely to have plate tectonics on super-Earth exoplanets. However, it cannot be ruled out due to large uncertainties in modeling and the lack of experimental data on core/mantle materials at pressures higher than experienced at the center of Earth (Stamenković et al. 2011).

As both the sinks and the sources of $CO_2$ are highly uncertain on exoplanets, it is not

possible to self-consistently calculate the atmospheric $CO_2$ level on an exoplanet different from Earth. Therefore, the $CO_2$ mixing ratio is a free parameter in our study. The mixing ratio of $CO_2$ is varied between $10^{-5}$ and $10^{-2}$. Large mixing ratio is expected, if plate tectonics is present on the exoplanet, because there is a stable source of $CO_2$. However, the sink of $CO_2$, liquid water precipitation is expected to be less efficient than on Earth because of the low relative humidities on hot desert worlds. The atmospheric $CO_2$ level is expected to be small, if plate tectonics does not operate on the exoplanet, because the mantle becomes depleted in carbon on a billion year timescale, and liquid precipitation in combination with surface weathering removes $CO_2$ from the atmosphere.

**Relative humidity** The relative humidity is a key parameter in our study because it has a strong influence on the inner edge distance. Unfortunately it is exceedingly difficult to model the relative humidity profile of an exoplanet because it is determined by complex 3D processes such as atmospheric circulation, cloud formation, precipitation. The water cycle is also influenced by the spatial distribution of liquid water on the planetary surface. We do not attempt to model these effects. However, we highlight some crucial aspects of the water cycle, and provide qualitative arguments on the requirements for low tropospheric relative humidity.

Strong temperature differences are necessary to maintain low relative humidity in the troposphere. The source of water vapor in the atmosphere is evaporation from a surface liquid reservoir, the sink of water vapor is condensation followed by precipitation. If precipitation does not reach the surface, the atmosphere eventually becomes fully saturated even if the fraction of surface liquids is small. Condensation and precipitation is initiated by cooling atmospheric parcels to saturation. Therefore, low relative humidity can be maintained, if strong temperature differences exist in the troposphere either vertically or horizontally. We argue that horizontal temperature differences are more important, because

if an air parcel is advected horizontally to cooler regions (night side or poles), rain drops surely reach the surface. However, if a rising air parcel e.g., in the Hadley circulation becomes saturated and rain drops form, it is not guaranteed that those drops reach the surface. The drops could evaporate as they fall through gradually warmer and drier regions of the troposphere (i.e., virga).

We show in Sect. 2.4 that the lower limit of plausible relative humidity is $\Phi \sim 1\%$. The lower limit is set by the required presence of liquid precipitation on the planet to wash out $CO_2$ from the atmosphere. If the relative humidity is $\Phi < 1\%$, the temperature difference necessary to cause precipitation is too large, and precipitation occurs in the form of snow. Solid precipitation above the freezing point of $CO_2$ is not able to remove $CO_2$ from the atmosphere, thus the $CO_2$ level and the surface temperature would rise on such a planet. We find that the temperature difference is safely in the liquid water precipitation range for all atmosphere types considered in this work, if the relative humidity is $\Phi = 1\%$.

**Surface temperature** The surface temperature at the inner edge of the Habitable Zone is determined by the surface pressure and the relative humidity. Traditionally the HZ is defined by the presence of liquid water on the surface. Therefore the inner edge temperature is given by the boiling point of water:

$$T_{\rm surf} = \max(T : P_{\rm surf} + \Phi P_{\rm sat}(T) > P_{\rm sat}(T)\,), \tag{5}$$

where $P_{\rm surf}$ is the dry surface pressure, $\Phi P_{\rm sat}(T)$ is the partial pressure of water on the surface. The inner edge surface temperature of Earth is 410 K for a dry surface pressure of 1 bar, and the surface relative humidity is 70%. If Earth had 1% relative humidity and all other properties kept constant, the inner edge surface temperature would be lower, 373 K because the partial pressure of water is reduced.

The maximum surface temperature is limited by the chemical stability of complex

organic molecules. If only Eq. 5 is used to calculate the inner edge surface temperature, its allowed range is between 273 K and 647 K given by the triple and critical points of water, respectively. However, can life exist at temperatures as high as 647 K? On Earth, organisms grow at temperatures up to 395 K (Kashefi & Lovley 2003; Takai et al. 2008). However, the DNA and amino acids become chemically unstable only at temperatures above 500 K (Lang 1986). Therefore we limit the surface temperature to a maximum of 500 K. We note that this is a globally averaged surface temperature because we use a 1D climate model. As discussed in the previous paragraph and in Sect. 2.4, large horizontal temperature differences are a requirement to initiate precipitation. Therefore the surface temperature at a substantial part of the planet must remain well below 500 K (see Sect. 2.4).

**Surface albedo** We assume that our exoplanets are hot and dry, thus most of the surface at low zenith angles is possibly covered by deserts or barren rocky surfaces. The surface albedo of Earth is 0.15 (Chapter 5 of Pierrehumbert 2011, based on ERBE measurements), and the main contributors are water, land, vegetation, and ice/snow surfaces. The albedo of the Sahara is 0.4 (Tetzlaff 1983), the albedo of water is 0.05 (Clark et al. 2007) We do not expect large water-covered areas on hot desert worlds, therefore we expect surface albedos between 0.05 and 0.4. Our nominal value is 0.2, but we varied the surface albedo between 0 and 0.6. We find that although higher surface albedos of low surface pressure atmospheres have an impact on the inner edge distance, the surface reflection becomes less important at high surface pressures because most of the incoming stellar flux is scattered back to space by Rayleigh scattering, or absorbed directly by the atmosphere. At 100 bars, typically less than 1% of the stellar flux reaches the surface. If the surface pressure is low, the surface albedo influences the tropopause height because the convective zone is driven by the absorption of stellar light at the surface.

**Nominal parameter values** The parameter values of our nominal simulation is shown in Table 1. The most important effect of these parameters is shown in Sect. 3. We typically change one parameter at a time, while the other parameters are held fixed at the value given in Table 1.

Table 1: Overview of parameter values in the nominal simulation.

| Parameter | Value |
|---|---|
| surface gravity | $g_{\rm surf} = 25$ m/s$^2$ |
| surface pressure | $P_{\rm surf} = 1$ bar |
| $CO_2$ mixing ratio | $X_{CO_2} = 10^{-4}$ |
| relative humidity | $\Phi = 1\%$ |
| surface temperature | $T_{\rm surf} = 370$ K [2] |
| surface albedo | $a_{\rm surf} = 0.2$ |
| background gas | $N_2$ |

### 2.4. The interplay of atmospheric circulation, and the hydrological cycle

As discussed previously, liquid water precipitation is crucial for two reasons: to keep the relative humidity of the atmosphere low, and to reduce the atmospheric $CO_2$ levels. An air parcel has to be cooled down to saturation to initiate condensation and precipitation. Therefore, the goal of this section is to study atmospheric circulation processes that can cause strong temperature differences. We distinguish two limiting cases: slowly rotating and/or tidally locked planets, and fast rotators like Earth. The distinction is necessary because different circulation regimes dominate the heat transfer depending on the rotation

[2]The surface temperature is a function of relative humidity and surface pressure.

period.

The dew point temperature ($T_d$) necessary to initiate condensation and precipitation is given by the globally averaged temperature of the air above the surface and the relative humidity. As a point of reference, if the globally averaged surface temperature is 370 K, and the relative humidity is 1%, the parcel has to cool down to $T_d = 280$ K to reach saturation. The dew point temperature for the same relative humidity value is 337 K, if the surface temperature is 500 K. Dew point temperatures above 273 K ensure that liquid water precipitation is present on the planet to act as a sink for atmospheric $CO_2$.

Cloud formation by vertical mixing is not considered because precipitation from cumulus clouds might not reach the surface (i.e., virga). If condensation occurred e.g., on the upwelling part of the Hadley circulation around the equator, it is uncertain whether rain drops reach the surface. It is likely that the drops evaporate as they fall through gradually warmer and drier regions of the troposphere.

### *2.4.1. Slow rotators and tidally locked planets*

The equator-to-pole temperature difference is typically small on planets with long periods (several tens to hundreds of days) because the Hadley cell extends all the way to the poles. As Hadley circulation transports heat very efficiently, the equator-to-pole temperature difference is expected to be small (Held & Hou 1980; Showman et al. 2011). However, the day-night temperature difference can be significant, if the atmosphere efficiently cools on the night side.

The speed of the zonal surface winds and the radiative cooling timescale determine the day-night temperature difference. Using the dew point temperature ($T_d$), and the radiative cooling timescale of the atmosphere, the zonal advection timescale is estimated

(Showman & Guillot 2002, Eq. 11):

$$\tau_{\rm zonal} = -\tau_{\rm rad} \log \left( 1 - \frac{T_{\rm surf} - T_d}{T_{\rm surf}} \right), \tag{6}$$

where $\tau_{\rm rad}$ is the radiative timescale of the atmosphere:

$$\tau_{\rm rad} = \frac{\Delta P}{g_{\rm surf}} \frac{c_p}{4\sigma T_{\rm surf}^3}, \tag{7}$$

where $\Delta P$ is the pressure difference at the top and bottom of the layer above the surface, $c_p$ is the heat capacity of the layer, and $\sigma$ is the Boltzmann constant. The zonal wind speed necessary to reach $T_d$ is

$$u_{\rm zonal} = R_p / \tau_{\rm zonal}, \tag{8}$$

where $R_p$ is the planet radius. As the required temperature difference is large ($\sim$100 K), it is necessary to have a small wind speed to preserve the large temperature contrast – although temperature differences drive winds. Therefore, we rejects exoplanet scenarios for which the estimated zonal wind necessary to preserve the required temperature difference is too small and use the mean surface wind speed of Earth as a reference value (7 m/s, Capps & Zender 2008).

### *2.4.2. Fast rotators*

The day-night temperature difference on fast rotators is small, but the equator-to-pole temperature difference can be significant. The Hadley cell cannot extend all the way to the poles on fast rotators, such as Earth (Held & Hou 1980). Instead, heat is transported from the maximum latitude of the Hadley cell to the poles by baroclinic instability (Stone 1978). In energy balance models, baroclinic instability is approximated as a large scale diffusion process (see e.g., Held 1999; Spiegel et al. 2008). We also take advantage of this formalism and calculate the diffusion coefficient necessary to create the equator-to-pole temperature difference of $T_{\rm surf} - T_d$.

The diffusion equation of the energy balance model is (Showman et al. 2011):

$$c_p \frac{\partial T(\phi)}{\partial t} = \nabla(c_p D \Delta T) + S(\alpha, \phi) - OTE, \tag{9}$$

where $T(\phi)$ is the temperature as a function of latitude, $D$ is the diffusion coefficient, and $S(\alpha, \phi)$ is the absorbed stellar flux as a function of latitude. An analytical solution exists for Eq. 9, if the albedo, $D$, $c_p$ are constants, the $OTE$ is fitted as $A + BT$, and if the stellar flux is parameterized as a constant plus a term proportional to the Legendre polynomial $P_2(\cos(\phi))$ (Held 1999). The diffusion coefficient expressed from the analytical solution is:

$$D = \frac{\left(\frac{T_{\rm surf}}{T_{\rm surf} - T_d} - 1\right) B R_p^2}{6 c_p}. \tag{10}$$

The parameter $B$ is determined by calculating radiative-convective equilibrium profiles with surface temperatures 1 K above and below the nominal $T_{\rm surf}$, and fitting the $OTE$. Our reference value for $D$ is the diffusion coefficient that reproduces the zonally averaged equator-to-pole temperature profile of Earth ($10^6$ m$^2$/s, Suarez & Held 1979). If an atmospheric scenario requires $D < 10^6$ m$^2$/s to preserve the necessary temperature difference, we reject the scenario.

### 2.5. The loss timescale of surface waters

The water reservoir of the planet is gradually depleted because the stellar UV radiation dissociates the stratospheric water vapor, and hydrogen subsequently escapes to space. The goal of this section is to estimate the loss timescale of the exoplanet's liquid reservoir assuming diffusion-limited escape. If the water loss time is too short, the planet could loose its water reservoir before life develops. On the other hand, if the timescale is on the order of several billion years, it is safe to assume that the surface waters are stable and long-lasting.

The most important reason to calculate radiative-convective T-P profiles is to reliably estimate the stratospheric water mixing ratio and through that the diffusion-limited escape

of $H_2O$. The tropopause pressure, temperature and relative humidity set the stratospheric water mixing ratio. It is expected that both the tropopause pressure and temperature varies with atmospheric and stellar parameters. Often it is assumed that the stratosphere has a constant 200 K temperature (Kasting et al. 1993; Kopparapu et al. 2013). However, the water loss timescale might be inaccurate as the tropopause properties are not self-consistently calculated. We note that a constant 200 K stratosphere temperature is small enough not to significantly affect the $OTE$ and thus the radiative equilibrium distance of the planet.

We assume that our hot desert worlds have a 100 times smaller liquid water reservoir than Earth, thus the total mass of liquid water reservoir is $1.4 \times 10^{22}$ g, which amounts to $N_{\rm H_2O} = 4.6 \times 10^{44}$ $H_2O$ molecules. The water loss timescale is calculated as

$$\tau_w = \frac{N_{\rm H_2O}}{A_{\rm surf} n^{\rm top}_{\rm H_2O} V_{\rm diff}}, \tag{11}$$

where $A_{\rm surf}$ is the surface area of the exoplanet, $n^{\rm top}_{\rm H_2O}$ is the number density of $H_2O$ molecules at the top of the atmosphere, and $V_{\rm diff}$ is the diffusion velocity calculated according to Hu et al. (2012). If the top-of-atmosphere temperature is 200 K, and the water vapor mixing ratio is $3 \times 10^{-5}$ on a planet with 10 m/s$^2$ surface gravity and one Earth radius, the water loss timescale is $5.2 \times 10^9$ years, in close agreement with the calculations of Kasting et al. (1993); Kopparapu et al. (2013).

## 3. Results

Our most significant finding is that exoplanets can be habitable much closer to the host star than previously estimated. For example, an exoplanet can be habitable as close as 0.5 AU from a solar-like star given favorable atmospheric properties. Hot and dry desert worlds with 1% relative humidity, a broad range of $CO_2$ mixing ratios and surface pressures, have

sufficiently long water loss timescales, such that surface liquid waters would continuously be present. The atmospheric circulation estimates also confirm this finding: the liquid water cycle can plausibly operate under a variety of atmosphere scenarios, thus $CO_2$ is washed out of the atmosphere, and the relative humidity is kept low. In other words, a variety of atmospheres could keep a planet habitable at the inner edge.

### 3.1. Relative humidity as the main controlling factor

The inner edge of the Habitable Zone can be as close as 0.5 AU around a solar-like star. The relative humidity of the atmosphere is the most important factor controlling how close a planet can be to a star and still maintain surface liquid water. The relative humidity can be as low as 1%, a plausible minimum for the liquid water cycle to operate (as shown in Sec. 2.4). If the relative humidity is lower than 1%, the necessary temperature difference (from day to night side or from equator to pole) to initiate condensation would be too high and precipitation would occur in the form of snow instead of rain on the night side. As snow is not able to wash out $CO_2$ from the atmosphere, $CO_2$ would accumulate and a planet with volcanism would develop a strong greenhouse effect like the Venusian atmosphere. The habitable zone for planets of 1% and higher humidity levels is shown in Fig. 1. In the following we discuss the top of atmosphere radiative properties of the atmosphere: the outgoing thermal emission (OTE) and the albedo of the planet.

The inner edge distance is close to the host star mainly because the outgoing thermal emission is high if the atmosphere is dry. In other words, the emitted thermal radiation escapes easily, if the greenhouse gas concentrations are low. The $OTE$ does not depend on the stellar type (see Fig. 2a); it is mainly influenced by the pressure-temperature profile and the greenhouse gas concentrations (shown in Fig. 3 for the nominal atmosphere of Table 1).

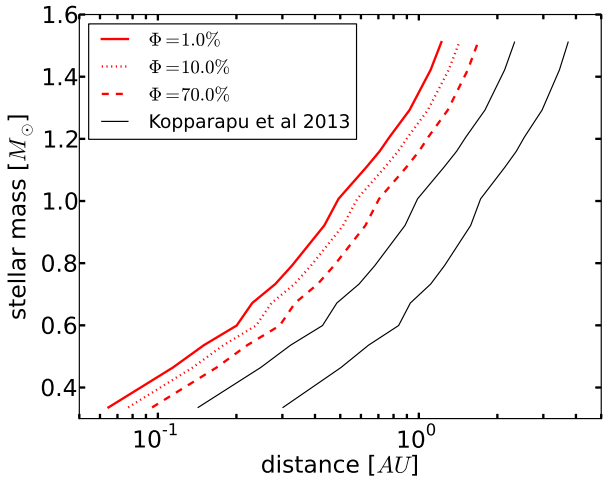


Fig. 1.— The inner edge of the Habitable Zone as a function of relative humidity. Other atmospheric parameters are fixed at the values given in Table 1. The x axis represents the planet-star separation, the y axis shows the mass of the host star. The inner edge distance is small for low relative humidity. The Habitable Zone limits of Kopparapu et al. (2013) are indicated with black solid lines.

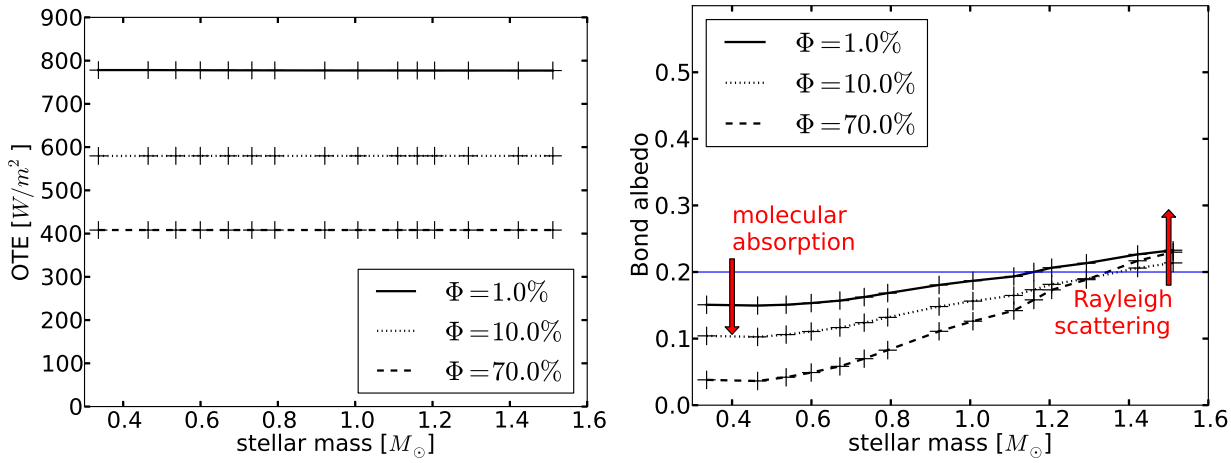


Fig. 2.— *Left:* The outgoing thermal flux as a function of relative humidity. The x axis shows the mass of the host star. *Right:* The Bond albedo of exoplanets as a function of relative humidity. The blue solid line indicates the surface albedo of 0.2.

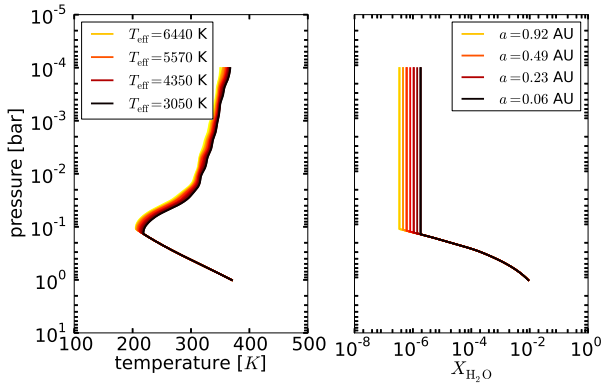


Fig. 3.— The temperature and water mixing ratio profiles of the nominal atmosphere with parameters given in Table 1. The color coding represents the T-P and water mixing ratio profiles of exoplanets orbiting various host stars. The effective temperatures of four selected host stars are indicated in the legend on the left side. The legend on the right side shows the equilibrium distance of the exoplanet around the host stars. The color coding is identical on all figures showing T-P and water mixing ratio profiles.

The second factor influencing the inner edge distance is the albedo of the planet. The planetary albedo is strongly influenced by the host star's spectral energy distribution, and the relative humidity (Marley et al. 1999). Low mass stars radiate at long wavelengths where absorption by greenhouse gases such as water and $CO_2$ is present. Therefore, the incoming stellar light is taken up by the atmosphere before it reaches the surface. The larger the relative humidity, the more stellar light is absorbed (see Fig. 2b). On the other hand, massive stars radiate at short wavelengths where Rayleigh scattering dominates. Therefore the planetary albedo around massive stars is typically larger than the surface albedo.

### 3.2. $CO_2$ mixing ratio influencing the water loss timescale

The atmospheric $CO_2$ mixing ratio influences the inner edge distance, which itself indirectly affects the water loss timescale. We discuss the effects of $CO_2$ on habitability from two perspectives: in this work, changes in the $CO_2$ level modifies the planet's radiative equilibrium distance (aka. the inner edge distance) because the surface temperature is fixed; the other perspective is to fix the planet's semi-major axis and investigate the influence of $CO_2$ on the climate. We shortly discuss the second perspective at the end of this section.

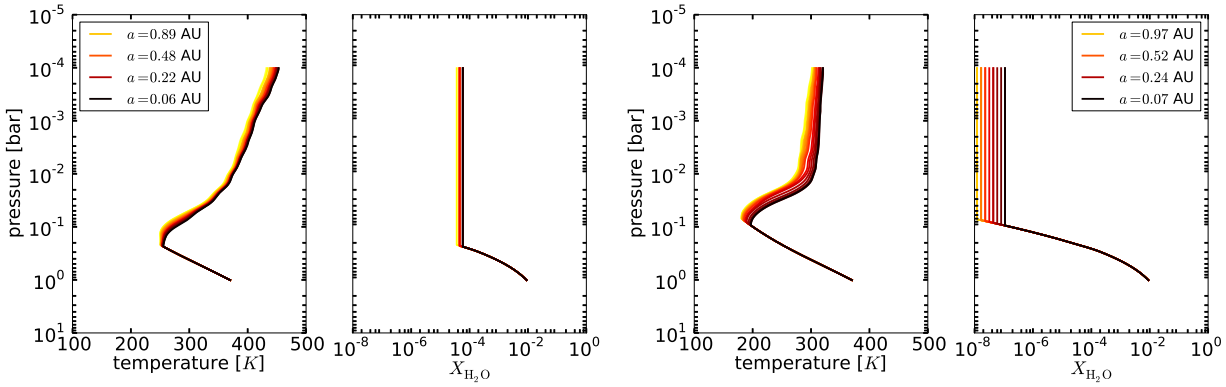


Fig. 4.— *Left:* The temperature and water mixing ratio profiles for a $CO_2$ mixing ratio of $10^{-5}$ with 1 bar surface pressure, 1% relative humidity. *Right:* The temperature-pressure and water mixing ratio profiles for a $CO_2$ mixing ratio of $10^{-2}$, other atmospheric parameters are unchanged. Higher levels of $CO_2$ results in colder tropopause temperatures, and dryer stratospheres at the inner edge. The color coding is identical as in Fig. 3.

The inner edge distance of planets with $CO_2$-rich atmospheres is large. The already knownreason is that $CO_2$ is a potent greenhouse gas, thus the outgoing thermal emission decreases with higher $CO_2$ levels. For example, the $OTE$ is 800 W/m$^2$ and 700 W/m$^2$ for $X_{CO_2} = 10^{-5}$ and $10^{-2}$, respectively. However, the albedo remains largely unaffected. As a result, the inner edge distance is 0.48 AU, and 0.52 AU for $CO_2$ mixing ratios of $10^{-5}$ and $10^{-2}$ around a solar-like star.

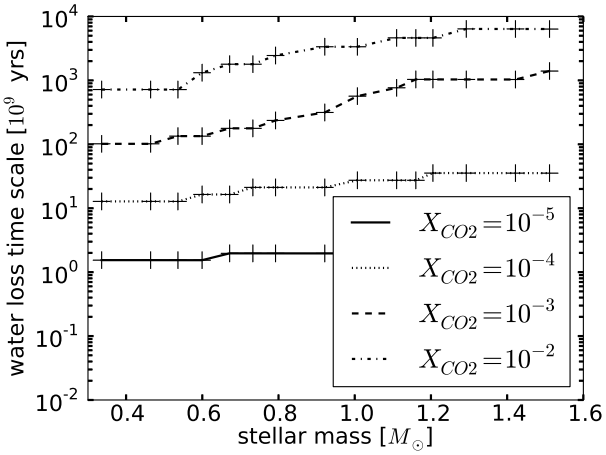


Fig. 5.— The water loss timescale at the inner edge as a function of $CO_2$ mixing ratio for atmospheres of 1% relative humidity and 1 bar surface pressure (for other parameters, see Table 1). As the stratospheric water levels are higher for low $CO_2$ mixing ratios (see Fig. 4), the water loss timescale becomes shorter. If the $CO_2$ mixing ratio is less than $10^{-4}$, the water loss timescale becomes shorter than 10 billion years.

The tropopause and stratosphere of exoplanets at the inner edge with low levels of atmospheric $CO_2$ are warm (see Fig. 4). This effect is explained by the variation of the inner edge distance with the $CO_2$ mixing ratio. Close-in planets are strongly illuminated, therefore the tropopause and the stratosphere are warm. The tropopause temperature is 240 K and 190 K for $CO_2$ levels of $10^{-5}$ and $10^{-2}$.

Close-in planets with low levels of $CO_2$ might quickly lose their surface waters and become inhabitable. The water loss timescale as a function of $CO_2$ mixing ratio is shown in Fig. 5. For a fixed relative humidity, the tropopause temperature determines the water-loss timescale (see Sect. 2.1). As discussed in the previous paragraph, the troposphere is cold, if the atmosphere is $CO_2$-rich at the inner edge. Therefore, the atmospheric $CO_2$ level has an indirect influence on the water loss timescale, because it regulates the tropopause temperature.

We note that for a fixed semi-major axis, the $CO_2$ mixing ratio has an opposite (but small) effect on the water loss timescale. Radiative-convective models of Earth's atmosphere show that doubling the atmospheric $CO_2$ warms the surface but slightly cools the tropopause (Schlesinger & Mitchell 1987). The result is that the stratospheric water mixing ratio reduces, and the water loss timescale is prolonged.

### 3.3. Intermediate surface pressure necessary for habitability on dry planets

The impact of surface pressure on habitability and the inner edge distance is complex.

Low surface pressures ($\sim$0.1 bar) are a problem because the water loss timescale is short and complex life might not have enough time to evolve (see Fig. 6). The water loss timescale of a hot desert world is only 0.1 billion years if the surface pressure is 0.1 bar, this is because the troposphere is confined to low altitudes, and the tropopause temperature only slightly differs from the surface temperature (see Fig. 7a). Therefore the stratosphere is water rich and the water loss timescale is short. At large surface pressures, the troposphere is extended, the tropopause is cold (see Fig. 7b), and the water loss timescale is always in excess of 10 billion years (see Fig. 6).

High surface pressures (100 bars) on tidally locked planets or slow rotators are problematic for habitability. The liquid water cycle cannot plausibly operate because the day-night side temperature difference is too low to initiate condensation. The rotation period of the exoplanet is an important factor influencing the water cycle because it prescribes the dominant circulation mode that redistributes heat. On tidally locked planets or slow rotators, heat from the day side is transported by zonal flows to the night side (see Sect. 2.4.1). If the surface pressure is 100 bars, the radiative cooling timescale of the atmosphere is long compared to the advection timescale. That is to say, an atmospheric

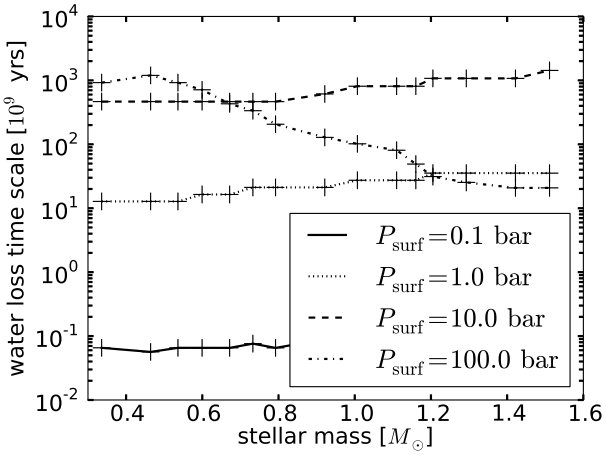


Fig. 6.— The water loss timescale at the inner edge as a function of surface pressure (see Table 1 for other parameters). The water loss timescale is above 10 billion years for all pressure values, if the $CO_2$ mixing ratio is $10^{-4}$.

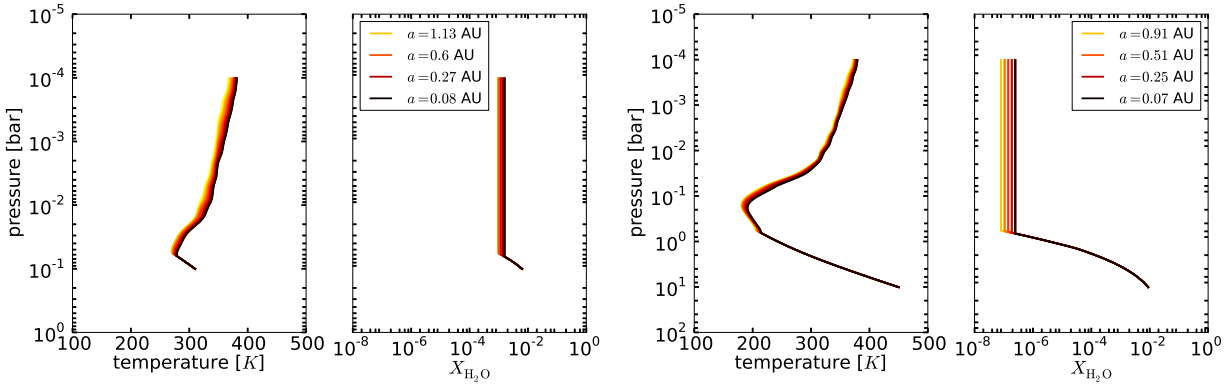


Fig. 7.— *Left:* The temperature and water mixing ratio profiles for an atmosphere with 0.1 bar surface pressure. Other parameters are given in Table 1. *Right:* Atmospheric profiles for a hot desert world with 10 bar surface pressure. The tropopause is much colder in this case. The color coding is identical as in Fig. 3.

parcel travels across the night side of the planet before it can cool down to the dew point temperature. To give a more qualitative argument, we calculate the surface zonal wind speed necessary to initiate condensation on the night side (Eq. 8). The zonal wind speed is

on the order of 1000 m/s, 100 m/s, 10 m/s, and 1 m/s for $P_{surf}$ = 0.1, 1, 10, and 100 bars, respectively. The inverse correlation between surface pressure and zonal wind speed is due to the long radiative cooling timescale at large pressures. The necessary zonal wind speed on exoplanets with 100 bars of surface pressure is too low, therefore, such atmospheres cannot plausibly cool down to the dew point temperature on the night side, and water condensation does not occur. On fast rotators like Earth, baroclinic instability transports heat from the equatorial regions to the poles (see Sect. 2.4.2). We find that the baroclinic diffusion coefficient required to initiate condensation around the poles (Eq. 10) is on the order of $10^{10}$ - $10^{11}$ $m^2/s$ for all surface pressures considered. These values are 4-5 orders of magnitude larger than the baroclinic diffusion coefficient on Earth. Therefore large equator to pole temperature differences and liquid precipitation are plausible on fast rotators at all surface pressures. The baroclinic diffusion coefficient is large because the $OTE$ changes rapidly as a function of surface temperature in dry and hot atmospheres (parameter B in Eq. 10).

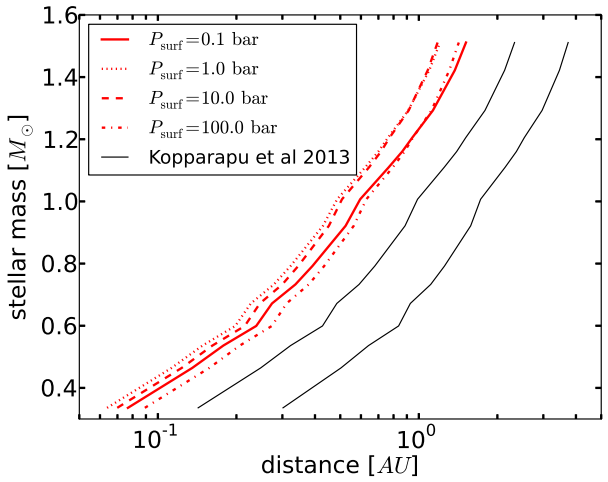


Fig. 8.— The inner edge of the Habitable Zone as a function of surface pressure. The inner edge moves further away from the host star with increasing surface pressures. The Habitable Zone limits of Kopparapu et al. (2013) are indicated with black solid lines.

A habitable planet with the smallest semi-major axis should have a surface pressure around 1 bar for stars less massive than 1.2 $M_\odot$, and a surface pressure of 10 bars around stars more massive than 1.2 $M_\odot$ (Fig. 8). The inner edge distance is a non-linear function of the surface pressure and the host star properties, because both the $OTE$ and the albedo show complex features (Fig. 9). The $OTE$ is maximized if the surface pressure is 1 bar. However, water boils at low temperatures, if the pressure is reduced. Therefore the surface temperature and thus the $OTE$ are small at low pressures. Although the boiling point and the surface temperature are high at large pressures, the optically thick atmosphere reduces the $OTE$ at large pressures (see Fig. 9a). The albedo of low pressure exoplanets is very close to the surface albedo. On the other hand, exoplanets with large surface pressures (100 bars) simultaneously have the lowest albedo around low mass stars due to greenhouse gas absorption; and they also have the highest albedo around massive stars due to Rayleigh scattering (Fig. 9b).

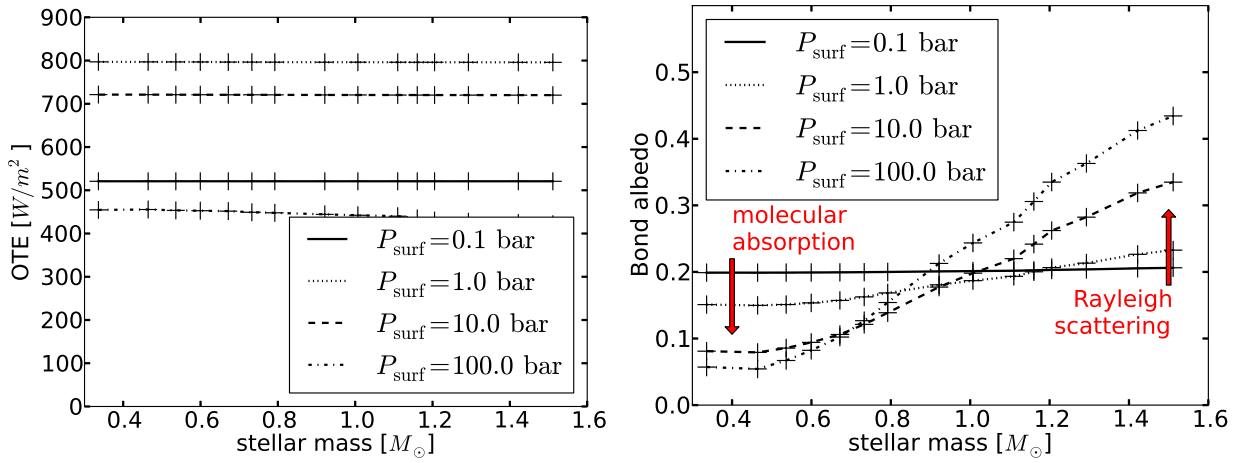


Fig. 9.— *Left:* The outgoing thermal flux as a function of surface pressure. *Right:* The Bond albedo of exoplanets as a function of surface pressure. The x axis shows the mass of the host star.

An exoplanet's surface pressure is actually difficult to ascertain whether it be a priori

from theory or from observations. The surface pressure of exoplanets is influenced by processes such as accretion from the protoplanetary disk, atmospheric escape, atmosphere accretion and/or erosion during impacts, and outgassing. In fact, the most challenging problem in proving that an exoplanet is habitable will be to observationally constrain its surface pressure. Even if the atmosphere is cloud-free, the atmosphere could be so optically thick that the surface remains hidden and unconstrained.

### 3.4. Surface gravity weakly influences the inner edge

The effect of the planet mass and radius on the inner edge distance is small compared to other factors discussed previously (see Fig. 10). Surface gravity influences the pressure scale height of the atmosphere and thus the column density of gases for a fixed surface pressure. The atmosphere of a Mars-sized small planet is expanded and thus the column density of all gases is raised. This has implications for the $OTE$ as well as the planetary albedo. Increasing the greenhouse gas column density reduces the $OTE$ from 800 W/m$^2$ to 700 W/m$^2$ for planets with surface gravities of 25 m/s$^2$ and 5 m/s$^2$, respectively. The albedo of a Mars-sized small planet shows the largest deviation from the surface albedo (see Fig. 11). The albedo around low mass stars is the lowest for small planets, because the greenhouse gas column density is large and the incoming stellar light is absorbed. At the same time, the albedo around massive stars is also the largest for small planets because Rayleigh scattering is more efficient due to the large column density of $N_2$.

Although the differences are small, the inner edge is slightly closer to the host star for super-Earth planets (see Fig. 8b). The distance around a solar-like star is 0.49 AU, 0.5 AU, and 0.51 AU for surface gravities of 5, 10, and 25 m/s$^2$. As the inner edge distance changes rather moderately with planet mass and size, it is a good approximation to use one common inner edge limit for all super-Earth and Earth-like planets. In the following we

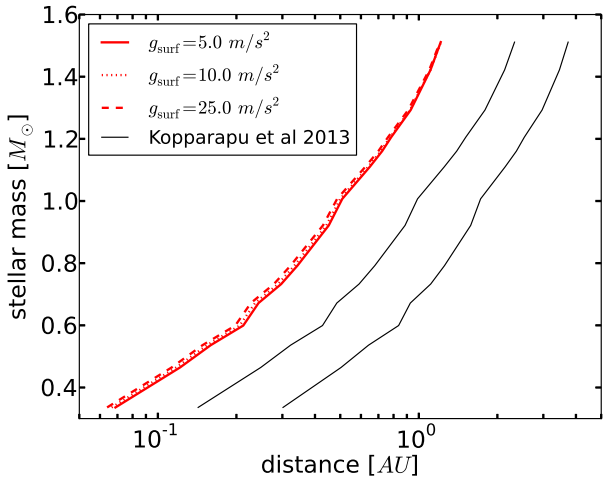


Fig. 10.— The inner edge of the Habitable Zone as a function of surface gravity. The x axis is the planet-star separation, the y axis shows the mass of the host star. Surface gravity has a small effect on the inner edge distance for the atmospheric configuration adapted. The inner edge is somewhat closer to the host star, if the surface gravity is small. The Habitable Zone limits of Kopparapu et al. (2013) are shown with black solid lines.

adopt the inner edge limit of the nominal atmosphere with properties outlined in Table 1).

### 3.5. Application to confirmed super-Earth exoplanets and candidates

We show semi-major axes and stellar masses of the currently confirmed and candidate super-Earth exoplanets in relation to our fundamental inner edge boundary and to the HZ limits of Kopparapu et al. (2013). We use the Open Exoplanet Catalogue of Rein (2012) as the source of stellar and exoplanetary data for confirmed exoplanets. The NASA Exoplanet Archive is used to access the Kepler exoplanet candidates of the Q1-Q8 data sets (Burke et al. 2013). If missing, the stellar mass is calculated using the empirical relations of Torres et al. (2010). We consider exoplanet (candidates) that have a mass (or $m \sin i$) less than 10 $M_{\rm Earth}$, and/or a radius less than 2.5 $R_{\rm Earth}$.

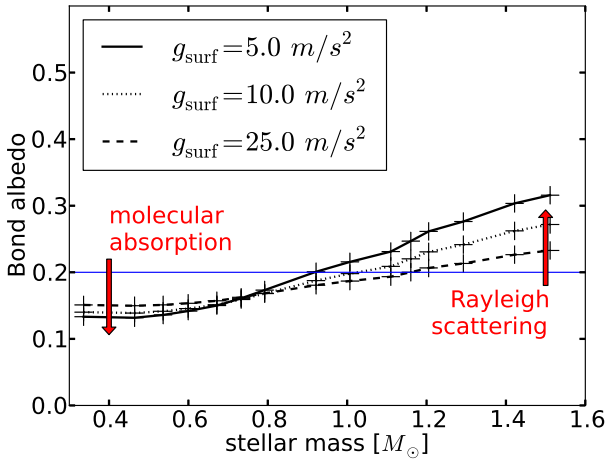


Fig. 11.— The Bond albedo of exoplanets as a function of surface gravity (other parameters given in Table 1). The outgoing thermal emission (not shown) is 700, 745, and 800 W/m$^2$ for surface gravities of 5, 10, and 25 m/s$^2$, respectively. As shown in Fig. 10, surface gravity has a modest influence on the inner edge distance.

There are nine radial velocity super-Earths, one confirmed transiting exoplanet, and one exoplanet discovered by microlensing that could potentially be habitable given suitable atmospheric conditions. The confirmed exoplanets are shown in Fig. 12a. The potentially habitable radial velocity planets with increasing host star mass are Gliese 581c, d, f, g (Udry et al. 2007, although the existence of Gliese 581 f and g are debated), Gliese 667Cc (Anglada-Escudé et al. 2012), HD 85512b (Pepe et al. 2011), HD 20794d (Pepe et al. 2011), HD 40307g (Tuomi et al. 2013), and tau Ceti d, e, and f (Tuomi et al. 2012). The transiting potentially habitable exoplanet is Kepler 22b (Borucki et al. 2012). The microlensing exoplanet OGLE-05-390L b (Beaulieu et al. 2006) could also be habitable, if its atmosphere is hydrogen-rich (Pierrehumbert & Gaidos 2011) or if it has a sufficient internal heat source (Rogers et al, in prep.).

We identify twenty potentially habitable Kepler candidates that have a radius below 2.5 $R_{\rm Earth}$. Their KOI IDs in order of increasing stellar mass are K01686.01, K00854.01,

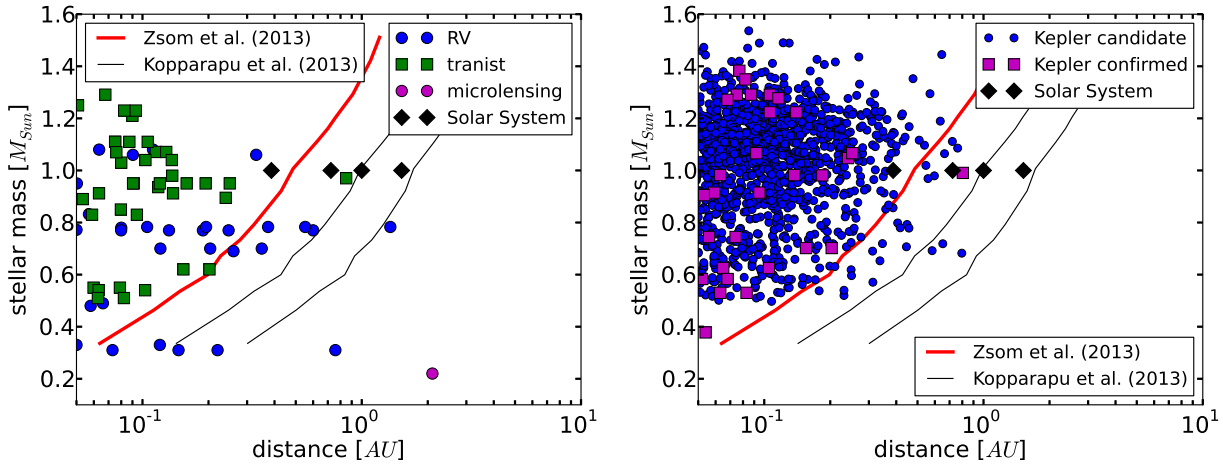


Fig. 12.— *Left:* The semi-major axes and stellar masses of confirmed super-Earth planets, and the fundamental inner edge of the Habitable Zone. Exoplanets discovered by various detection methods are included in the figure, as well as the Habitable Zone limits of Kopparapu et al. (2013), and the positions of the four rocky Solar System planets. *Right:* The Kepler confirmed and candidate super-Earth planets. The number of potentially habitable exoplanets increases by a factor of 2-3 compared to previous estimates. However, follow-up observations aimed to characterize super-Earth atmospheres are necessary to determine whether these exoplanets are really habitable.

K02418.01, K03010.01, K01361.01, K01298.02, K01174.01, K02882.01, K02770.01, K02762.01, K00518.03, K01871.01, K02834.01, K00701.03, K02469.01, K03036.01, K02474.01, K02311.01, K00172.02, and K01739.01. Although our minimum stellar mass is 0.33 $M_{\odot}$, Fig. 12b indicates that potentially habitable exoplanets are quite possibly teeming around low mass stars.

# 4. Discussion

## 4.1. The formation of desert worlds

Where should we look for hot desert worlds? Is it possible to estimate their occurrence rate? What factors play a significant role in forming desert worlds? To answer these questions, we rely on N-body simulations of interacting planetary embryos and planetesimals (e.g., Morbidelli et al. 2000; Chambers 2001; Raymond et al. 2004, 2006, 2007). Such models simulate how planetary embryos accrete water-rich km-sized planetesimals coming past the snow line.

Although it is currently not possible to estimate the occurrence rate of hot desert worlds, we infer from N-body simulations (e.g., Raymond et al. 2004) that metal poor and/or slowly rotating stars could preferentially host such planets. The most important factor influencing the water content of small exoplanets is the surface density of solids around the snow line. If the surface density is low, dry Earth-sized planets form. Two main factors influence the surface density of solids: the total disk mass, and the metallicity. The disk mass is influenced by the angular momentum of the protostellar core. If the core rotates slowly, most mass falls directly onto the protostar, and the disk mass remains moderate (e.g., Yorke et al. 1993; Matsumoto et al. 1997; Zhu et al. 2010). As angular momentum is conserved, a slowly rotating core produces a slowly rotating star. Thus the stellar rotation period might be indicative of the exoplanetary water content. Metallicity also influences the surface density of solids past the snow line. Thus hot desert worlds could preferentially form around low metallicity stars. The occurrence rate of low-mass planets does not seem to have a strong metallicity dependence (unlike for hot Jupiters Buchhave et al. 2012), but a statistical sample of characterized exoplanet atmospheres could in the future show us that the exoplanetary water or volatile content correlates with the metallicity.

### 4.2. Observables

Do desert worlds have a hallmark signature in their spectra? Can we identify a habitable desert world? The surface conditions (such as surface pressure, temperature, and the mixing ratio of atmospheric constituents) must be constrained by observations to unambiguously identify a habitable world. We use transmission spectroscopy to illustrate the difficulty in this process. We show the effective height (Kaltenegger & Traub 2009) of three types of atmospheres in Fig. 13: our nominal hot desert world with 10 $m/s^2$ surface gravity (Table 1); the effective height of a $CO_2$ dominated Venus-like atmosphere with a water mixing ratio of $3 \times 10^{-5}$; and the effective height of an Earth-like atmosphere with $N_2/CO_2/H_2O$ (other gases are removed for easy comparison). The spectra are computed at high resolution ($\lambda/\delta\lambda = 10^5$) and binned down to a resolution of 1000, which is comparable to the medium resolution of NIRSPEC on the James Webb Space Telescope (Bagnasco et al. 2007). The illustrated transmission signals are noise-free, but a typical signal-to-noise ratio is expected to be $\sim$10 for water features at 2 micron for systems out to 12 pc (Deming et al. 2009).

It might not be possible to identify a habitable exoplanet with certainty. The greatest challenge is to constrain the surface pressure and the mixing ratio of water in the surface regions. Water vapor is abundant in the atmosphere close to the surface, if a surface reservoir is present. However, transmission spectroscopy typically constrains the stratospheric mixing ratios only, because the surface region is expected to be optically thick at all wavelengths, and thus the transmission signal is, for the most part, unaffected by the troposphere. This is a problem, because the surface properties such as the surface pressure, and the water reservoir of the planet remain unconstrained by observations. This point is illustrated in Fig. 13 because the water features of a hot desert world and an Earth-like planet are similar, although the surface relative humidity differs by almost two

orders of magnitude. Furthermore, the effective height is above 5 km for both cases, thus the surface regions are unconstrained. The largest difference in the transmission signal is at wavelengths shorter than 1 micron, because this part of the spectrum is influenced by the pressure scale height of the atmosphere. The pressure scale height is

$$H_p = \frac{kT}{Mg_{\rm surf}}, \tag{12}$$

where $k$ is the Boltzmann constant, $T$ is the temperature of the atmosphere, and $M$ is the mean molecular mass. The mean molecular mass is similar in the two cases, the surface gravities are identical. However, the temperatures on a hot desert world are larger than on Earth. The average surface temperature of the hot desert world is 370 K in contrast to the 290 K surface temperature of Earth. The amplitude of the molecular features differs at all wavelengths. This difference is also explained by the large pressure scale height on hot desert worlds.

Although we might not be able to tell with certainty whether a planet is habitable, it will be possible to rule out inhabitable planets with confidence. If the stratospheric mixing ratios of $CO_2$ and water are retrievable from the transmission spectrum, it is possible to distinguish a $CO_2$-dominated atmosphere from an $N_2$-dominated atmosphere (Benneke & Seager 2012). Variations in the effective height are modest in a $CO_2$ dominated atmosphere for two reasons. First, the $CO_2$ absorption lines are wide and the atmosphere absorbs significantly even in between band center regions. Second, the scale height of a $CO_2$ dominated atmosphere is small because the molecular weight of $CO_2$ is larger than the molecular weight of $N_2$. However, if the $CO_2$ and water mixing ratios are small, the variations in effective height are large (see Fig. 13). Measuring the relative effective heights of band centers and window regions is a way to distinguish $CO_2$-dominated atmospheres from Earth-like and hot desert world atmospheres.

We emphasize the previously known result that the transmission signal of low surface

gravity planets is easier to detect because the atmosphere has a large scale height (Eq. 12), and thus the variations in the transmission signal are large. We illustrate the influence of surface gravity on the effective height for hot desert worlds in Fig. 14.

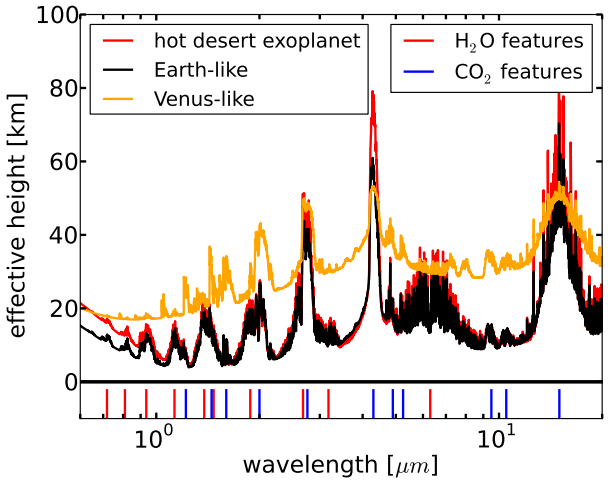


Fig. 13.— The effective height of a hot desert world with 10 m/s$^2$ surface gravity (other parameters in Table 1), Venus (with the 0 km height moved to 1 bar), and an Earth-like planet (with only $N_2$, water and $CO_2$ in the atmosphere). Medium resolution spectra obtained with the JWST will enable us to distinguish a hot desert world from a Venus-like atmosphere. The effective height of an Earth-like planet and a hot desert worlds look similar. The difference at short wavelength is due to the different scale heights of the atmospheres. However, the surface regions remain optically thick at all wavelengths.

## 4.3. Model uncertainties

### *4.3.1. Clouds*

The effects of clouds on the inner edge distance is presumably small, because we do not expect tenuous water clouds covering a large fraction of the surface on dry worlds. However, there are some cases where clouds could influence the inner edge distance. Most

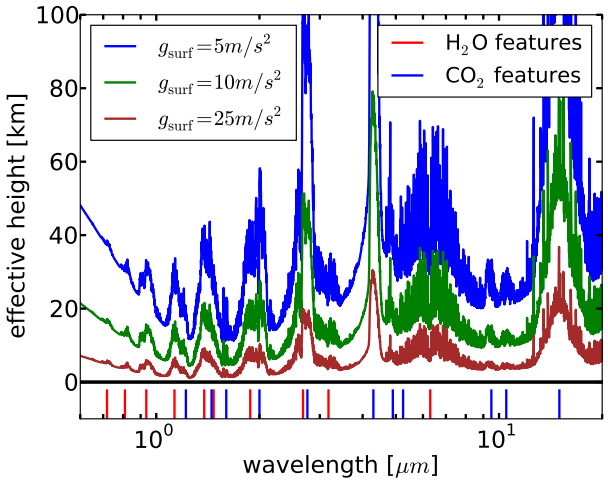


Fig. 14.— The effective height of hot desert worlds with various surface gravities (for other parameters, see Table 1). The surface gravity influences the pressure scale height of the atmosphere. The molecular features are easier to detect, if the exoplanet's surface gravity is small, thus the pressure scale height is large.

notable is clouds forming in the convective equatorial regions of the Hadley cell. Cloud formation is initiated by condensation, thus large surface-tropopause temperature difference is necessary to form convective clouds. The temperature difference is large, if the $CO_2$ mixing ratio and/or the surface pressure are large. Even if clouds do form, it is expected that clouds form high in the troposphere (Zsom et al. 2012), therefore the clouds might be thinner on hot desert worlds than on Earth. Furthermore, it is difficult to a priori estimate whether such clouds would reduce or increase the inner edge distance, because the albedo effect and the warming effect of high clouds is typically on the same order of magnitude (Goldblatt & Zahnle 2011).

Clouds forming on the night side of slow rotators could also influence the inner edge distance, if such clouds extend to the day side. If zonal winds shepherd clouds to the day side, and the clouds survive to the vicinity of the sub-stellar point, the albedo effect of

clouds could push the inner edge closer to the host star. Clouds form predominantly at the poles on fast rotators assuming that their rotation axis is close to perpendicular to the orbital plane, thus their effect on the inner edge distance is limited due to the large zenith angle of incoming stellar radiation.

### *4.3.2. 1D vs. 3D*

The main assumption in our approach is that the mixing ratio of atmospheric constituents and the temperature-pressure profile is described by 1D vertical globally averaged quantities. If the mixing ratio of a chemical is influenced by processes operating on short timescales relative to atmospheric mixing, spatial variations in mixing ratio throughout the atmosphere are expected to be large. $CO_2$ is assumed to be well-mixed because the carbon-silicate cycle operates on a long timescale (Walker et al. 1981). However, the mixing ratio of $H_2O$ could show large horizontal variations because the surface waters are expected to be confined to a small portion of the surface on hot desert worlds, and precipitation is not anticipated on the day side. Such mixing ratio variations could have important implications to planetary climate and the inner edge distance because regions with below average relative humidities act as global coolants. Two examples are the dry downwelling part of the Hadley cell or the Foehn wind. The optical depth in these columns is reduced and more infrared radiation escapes to space thus cooling the planet. Areas with above average relative humidities are expected where precipitation occurs (night side or poles). The enhanced greenhouse effect in these areas increases the cooling timescale of Eq. 7 thus reduce the overall horizontal temperature gradients. Multidimensional coupled radiative and circulation models are necessary to study these effects on the climate.

### *4.3.3. Relative humidity profile*

Other crucial assumption is the constant tropospheric relative humidity profile. The relative humidity profile determines the column density of water vapor in the troposphere and thus the radiative properties of the atmosphere. The relative humidity profile on Earth decreases with altitude being 70% on the surface and a couple of percentage at the tropopause (Manabe & Wetherald 1967). The relative humidity profile is determined by the water cycle: surface evaporation, atmospheric circulation, condensation, and precipitation. It is beyond the scope of this paper to study such effects, but we plan to investigate this problem in the future.

## 5. Summary and Conclusions

We studied atmospheric configurations that provide habitable surface conditions while minimizing the semi-major axis of the exoplanet. We recalled that liquid precipitation is a dominant removal process for atmospheric $CO_2$. Rain is also necessary to keep the relative humidity low because it acts as a sink for both water vapor and $CO_2$. Therefore, we provided a lower limit on relative humidity required for liquid precipitation. We studied the atmospheric circulation requirements to initiate condensation and precipitation either on the night side or at the poles of exoplanets. The water loss timescale was also estimated to assess the life-time of the surface water reservoir. Note that we focused exclusively on the inner edge of the Habitable Zone, because the outer edge extends well beyond the $N_2$-$O_2$ Habitable Zone limits of Kasting et al. (1993); Kopparapu et al. (2013) for $H_2$-He dominated atmospheres (Pierrehumbert & Gaidos 2011), or it can extend to infinity, if the exoplanet has a sufficient internal heat source (Rogers et al, in prep.).

Our main results are summarized here:

- We estimate that the fundamental inner edge of the Habitable Zone is at 0.5 - 0.6 AU around a solar-like star, well within the orbit of Venus for a variety of atmospheric scenarios.

- Planets with dry atmospheres are habitable close to the host star. We estimate that a relative humidity of 1% could be sufficient to initiate liquid water precipitation. If the relative humidity is smaller than 1%, precipitation might occur predominantly in the form of snow that is unable to remove $CO_2$ from the atmosphere if the temperature is above the freezing point of $CO_2$.

- The water loss timescale is longer than 10 billion years, if the atmospheric $CO_2$ level is above $10^{-4}$ and the surface pressure is more than 1 bar. As we argued in Sect. 2.3, if plate tectonics does not recycle carbon, the atmosphere and the mantle could be depleted in $CO_2$ on a billion year timescale, and carbon remains locked in the form of carbonates in shallow water regions. Therefore plate tectonics or other processes are necessary to either keep the $CO_2$ level balanced, or to reduce the stratospheric water mixing ratio by other means.

- If the surface pressure on slow rotators and tidally locked planets is on the order of 1-10 bars, it is plausible that zonal winds enable a cold night side (dew point) and precipitation. For large surface pressures (e.g., 100 bars), the heat capacity of the atmosphere is large and it prevents strong cooling and temperature differences.

- Liquid water precipitation is plausible at the poles of fast rotators, because the required baroclinic diffusion coefficient to initiate precipitation is large for all atmospheric scenarios considered here.

- The number of potentially habitable confirmed exoplanets increases by a factor of 2-3 as compared to Kopparapu et al. (2013). The potentially habitable exoplanets are

Gliese 581 d, e, f, Gliese 667Cc, Gliese 163c, HD 20794d, HD 40307g, tau Ceti d, e, f, and Kepler 22b.

- The surface regions are not constrained by transmission spectroscopy even though the water mixing ratio on hot desert worlds is smaller than on Earth.

The first confirmed habitable exoplanet will likely be a hot desert world – as introduced in this study – because it is easier to characterize their atmospheres. Such close-in exoplanets orbiting small stars have a large transit probability, and a large transit over rotation period ratio that increase the observational window for a given mission. Characterizing low mass desert worlds around nearby M dwarfs is especially likely because the atmospheric scale height increases for low-mass planets while the planet-to-star area ratio remains favorable. Therefore future modeling studies will aim to better understand the atmospheric circulation, the water cycle, and geophysical processes of such exoplanets. Observational campaigns conducted to characterize Earth-like exoplanet atmospheres should consider all super-Earth or Earth-sized exoplanets residing further out their host star than the fundamental inner edge limit.

A. Zsom is grateful for discussions with Nikole Lewis, Renyu Hu, Vlada Stamenkovic, Ramses Ramirez, Daniel James Cziczo, Ray Pierrehumbert, James Kasting, and Felipe Gerhard. A. Zsom was supported by the German Science Foundation (DFG) under grant ZS 107/2-1. J.d.W. acknowledges support from the B.A.E.F. (Belgian American Educational Foundation) in the form of a fellowship.

## A. Model validation

**Thermal emission** We compare our radiative transfer code against the radiative transfer (RT) module of the Community Climate Model (*ccm*3) of the National Center for Atmospheric Research (Kiehl et al. 1998). The *ccm*3 model was developed for climate change studies, thus its radiative transfer module is more accurate than our code in the temperature, pressure, water and $CO_2$ mixing ratio ranges typically encountered in the atmosphere of Earth. Several effects are included in the *ccm*3 RT model that we ignored to keep our code simple. Some of these effects are: properly treating overlapping lines of different absorbers (we use the assumption of random overlapping), calculating the IR flux in subdivided atmospheric layers to resolve the temperature gradient through the layer (we assume that the layers are isothermal). We show by the end of this section that ignoring these effects results in a relative error on the order of a few percent in the thermal IR fluxes.

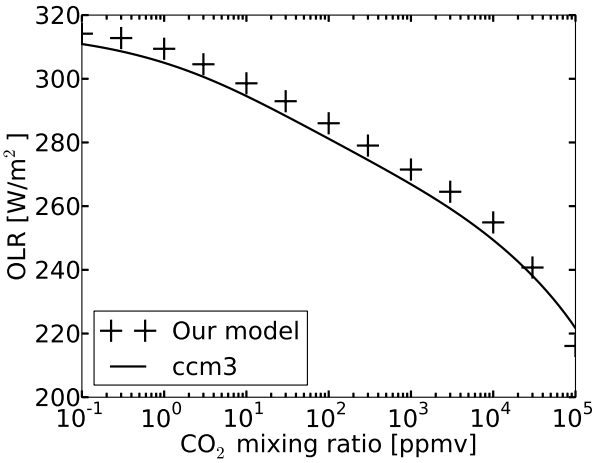


Fig. 15.— The outgoing thermal flux of a dry $N_2$-$O_2$ atmosphere with 1 bar surface pressure, 273 K surface temperature, and various $CO_2$ mixing ratios. The solid line represents calculations performed with the Community Climate Model (*ccm*3) of the National Center for Atmospheric Research. Thermal flux values calculated with our model are shown with '+' signs. The relative error between our results and the *ccm*3 model is below 2%.

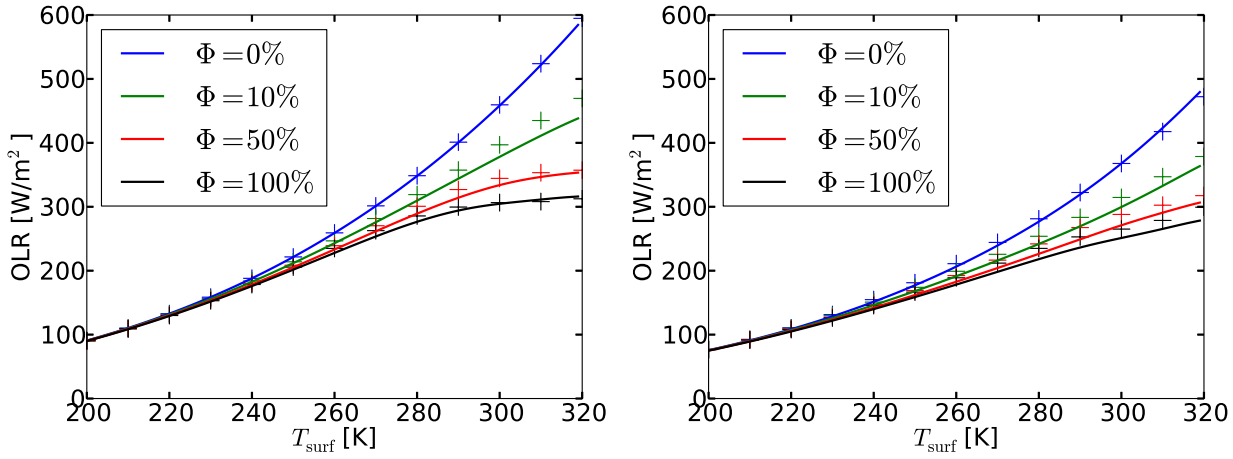


Fig. 16.— *Left:* The outgoing thermal flux of a moist adiabat atmosphere for four levels of relative humidity and various surface temperatures without $CO_2$. *Right:* The outgoing thermal flux of moist adiabat atmosphere profiles with $10^4$ ppmv $CO_2$ added. The solid lines correspond to *ccm*3 calculations, the '+' symbols show our results. The relative error is less than 7% in all cases.

We calculate the outgoing thermal emission ($OTE$) of all-troposphere atmospheres with various temperatures, relative humidities and $CO_2$ mixing ratios using our model and *ccm*3 RT. The first comparison is performed using a dry $N_2$-$O_2$ atmosphere with 273 K surface temperature and various $CO_2$ mixing ratios. The results are shown in Fig. 15. The solid line represents the *ccm*3 RT results, the '+' signs correspond to our calculations. Although our fluxes are typically larger than the *ccm*3 fluxes, the relative error between our results and *ccm*3 is less than 2%, thus our model agrees well with *ccm*3.

Next, the $OTE$ for an $N_2$-$O_2$ all-troposphere atmosphere is calculated with four different values of relative humidity: $\Phi$ = 0, 10, 50, and 100 %, but without $CO_2$ (see Fig. 16a). If the relative humidity is zero, there is no greenhouse gas in the atmosphere, thus the corresponding fluxes are generated by the black body emission of the surface. At surface temperature below 240 K, the water content of the atmosphere is so low that only a small

amount of the IR flux is held back. Fig. 16a shows how increasing the relative humidity lowers the outgoing thermal emission at the top of the atmosphere. The maximum relative error observed between our and the *ccm*3 fluxes is 7%, which we find acceptable.

The next level of complexity is to include both water vapor and $CO_2$ in the atmosphere. Fig. 16b shows the $OTE$ of the atmosphere profiles used in the previous paragraph with 1% $CO_2$ added. The outgoing thermal flux is significantly reduced by $CO_2$. As before, the maximum relative error is an acceptable 7%.

## REFERENCES

Abbot, D. S., Cowan, N. B., & Ciesla, F. J. 2012, ApJ, 756, 178

Abe, Y., Abe-Ouchi, A., Sleep, N. H., & Zahnle, K. J. 2011, Astrobiology, 11, 443

Anglada-Escudé, G., Arriagada, P., Vogt, S. S., et al. 2012, ApJ, 751, L16

Bagnasco, G., Kolm, M., Ferruit, P., et al. 2007, 66920M

Barnes, R., Mullins, K., Goldblatt, C., et al. 2012, ArXiv e-prints

Beaulieu, J.-P., Bennett, D. P., Fouqué, P., et al. 2006, Nature, 439, 437

Benneke, B., & Seager, S. 2012, ApJ, 753, 100

Bohren, C. F., & Huffman, D. R. 1983, Absorption and scattering of light by small particles (Wiley)

Borucki, W. J., Koch, D. G., Batalha, N., et al. 2012, ApJ, 745, 120

Borysow, A. 2002, A&A, 390, 779

Buchhave, L. A., Latham, D. W., Johansen, A., et al. 2012, Nature, 486, 375

Burke, C. J., Bryson, S., Christiansen, J., et al. 2013, in American Astronomical Society Meeting Abstracts, Vol. 221, American Astronomical Society Meeting Abstracts, 216.02

Capps, S. B., & Zender, C. S. 2008, Journal of Climate, 21, 6569

Castelli, F., & Kurucz, R. L. 2004, ArXiv Astrophysics e-prints

Chambers, J. E. 2001, Icarus, 152, 205

Clark, R., Swayze, G., Wise, R., et al. 2007, Usgs digital Spectral Library splib06a: US Geological Survey, Data Series 231

Coltice, N., Simon, L., & Lécuyer, C. 2004, Geophys. Res. Lett., 31, 5603

Deming, D., Seager, S., Winn, J., et al. 2009, PASP, 121, 952

Des Marais, D. J., Harwit, M. O., Jucks, K. W., et al. 2002, Astrobiology, 2, 153

Fujii, Y., Kawahara, H., Suto, Y., et al. 2011, ApJ, 738, 184

Goldblatt, C., & Watson, A. J. 2012, Royal Society of London Philosophical Transactions Series A, 370, 4197

Goldblatt, C., & Zahnle, K. J. 2011, Climate of the Past, 7, 203

Gruszka, M., & Borysow, A. 1997, Icarus, 129, 172

Harvey, A. H., Gallagher, J. S., & Levelt Sengers, J. M. H. 1998, Journal of Physical and Chemical Reference Data, 27, 761

Hegde, S., & Kaltenegger, L. 2013, Astrobiology, 13, 47

Held, I. M. 1999, Tellus Series A, 51, 59

Held, I. M., & Hou, A. Y. 1980, Journal of Atmospheric Sciences, 37, 515

Hu, R., Seager, S., & Bains, W. 2012, ApJ, 761, 166

Javoy, M., Pineau, F., & Allègre, C. J. 1982, Nature, 300, 171

Joshi, M. M., & Haberle, R. M. 2012, Astrobiology, 12, 3

Kaltenegger, L., & Sasselov, D. 2010, ApJ, 708, 1162

Kaltenegger, L., & Traub, W. A. 2009, ApJ, 698, 519

Kaltenegger, L., Selsis, F., Fridlund, M., et al. 2010, Astrobiology, 10, 89

Kashefi, K., & Lovley, D. R. 2003, Science, 301, 934

Kasting, J. F., Whitmire, D. P., & Reynolds, R. T. 1993, Icarus, 101, 108

Kiehl, J. T., Hack, J. J., Bonan, G. B., et al. 1998, Journal of Climate, 11, 1131

Kitzmann, D., Patzer, A. B. C., von Paris, P., et al. 2010, A&A, 511, A66+

Kopparapu, R. k., Ramirez, R., Kasting, J. F., et al. 2013, ArXiv e-prints

Lammer, H., Odert, P., Leitzinger, M., et al. 2009, A&A, 506, 399

Lang, E. 1986, Advances in Space Research, 6, 251

Liu, Y., Lin, J., Huang, G., Guo, Y., & Duan, C. 2001, Journal of the Optical Society of America B Optical Physics, 18, 666

Manabe, S., & Wetherald, R. T. 1967, Journal of Atmospheric Sciences, 24, 241

Marley, M. S., Gelino, C., Stephens, D., Lunine, J. I., & Freedman, R. 1999, ApJ, 513, 879

Matsumoto, T., Hanawa, T., & Nakamura, F. 1997, ApJ, 478, 569

Morbidelli, A., Chambers, J., Lunine, J. I., et al. 2000, Meteoritics and Planetary Science, 35, 1309

Olivero, J. 1977, J. Quant. Spec. Radiat. Transf., 17, 233

Pepe, F., Lovis, C., Ségransan, D., et al. 2011, A&A, 534, A58+

Pierrehumbert, R., & Gaidos, E. 2011, ApJ, 734, L13

Pierrehumbert, R. T. 2011, Principles of Planetary Climate (Cambridge Univ Pr)

Raymond, S. N., Quinn, T., & Lunine, J. I. 2004, Icarus, 168, 1

—. 2006, Icarus, 183, 265

Raymond, S. N., Scalo, J., & Meadows, V. S. 2007, ApJ, 669, 606

Rein, H. 2012, ArXiv e-prints

Rothman, L. S., Gordon, I. E., Barbe, A., et al. 2009, J. Quant. Spec. Radiat. Transf., 110, 533

Rugheimer, S., Kaltenegger, L., Zsom, A., Segura, A., & Sasselov, D. 2012, ArXiv e-prints

Sander, S. P., Friedl, R. R., Ravishankara, A. R., et al. 2006, NASA SLASH JPL Publication

Schlesinger, M. E., & Mitchell, J. F. B. 1987, Reviews of Geophysics, 25, 760

Seager, S., Turner, E. L., Schafer, J., & Ford, E. B. 2005, Astrobiology, 5, 372

Segura, A., Kasting, J. F., Meadows, V., et al. 2005, Astrobiology, 5, 706

Showman, A. P., Cho, J. Y.-K., & Menou, K. 2011, Exoplanets, ed. S. Seager & R. Dotson, Space Science (University of Arizona Press), 471–516

Showman, A. P., & Guillot, T. 2002, A&A, 385, 166

Sleep, N. H., & Zahnle, K. 2001, J. Geophys. Res., 106, 1373

Sneep, M., & Ubachs, W. 2005, J. Quant. Spec. Radiat. Transf., 92, 293

Spiegel, D. S., Menou, K., & Scharf, C. A. 2008, ApJ, 681, 1609

Stamenković, V., Breuer, D., & Spohn, T. 2011, Icarus, 216, 572

Sterzik, M. F., Bagnulo, S., & Palle, E. 2012, Nature, 483, 64

Stevenson, D. J. 1999, Nature, 400, 32

Stone, P. H. 1978, Journal of Atmospheric Sciences, 35, 561

Suarez, M. J., & Held, I. M. 1979, J. Geophys. Res., 84, 4825

Takai, K., Nakamura, K., Toki, T., et al. 2008, Proceedings of the National Academy of Sciences, 105, 10949

Tetzlaff, G. 1983, Albedo of the Sahara, Tech. rep., Technische Univ., Hanover (Germany)

Toon, O., McKay, C., Ackerman, T., & Santhanam, K. 1989, Journal of Geophysical Research, 94, 16287

Torres, G., Andersen, J., & Giménez, A. 2010, A&A Rev., 18, 67

Tuomi, M., Anglada-Escudé, G., Gerlach, E., et al. 2013, A&A, 549, A48

Tuomi, M., Jones, H. R. A., Jenkins, J. S., et al. 2012, ArXiv e-prints

Udry, S., Bonfils, X., Delfosse, X., et al. 2007, A&A, 469, L43

Vladilo, G., Murante, G., Silva, L., et al. 2013, ArXiv e-prints

Walker, J. C. G., Hays, P. B., & Kasting, J. F. 1981, J. Geophys. Res., 86, 9776

Weber, M. 2003, Handbook of Optical Materials, CRC Press Laser & Optical Science & Technology (CRC PressINC)

Wiscombe, W. J., & Evans, J. W. 1977, Journal of Computational Physics, 24, 416

Yorke, H. W., Bodenheimer, P., & Laughlin, G. 1993, ApJ, 411, 274

Zhu, Z., Hartmann, L., & Gammie, C. 2010, The Astrophysical Journal, 713, 1143

Zsom, A., Kaltenegger, L., & Goldblatt, C. 2012, Icarus, 221, 603